Fuel 222 (2018) 83–97

Contents lists available at ScienceDirect

Fuel

journal homepage: www.elsevier.com/locate/fuel

Full Length Article

Laboratory study of proppant on shale fracture permeability and compressibility

Yuling Tan[a,b,c], Zhejun Pan[c,*], Jishan Liu[d], Xia-Ting Feng[a,e], Luke D. Connell[c]

[a] State Key Laboratory of Geomechanics and Geotechnical Engineering, Institute of Rock and Soil Mechanics, Chinese Academy of Sciences, Wuhan, Hubei 430071, China
[b] University of Chinese Academy of Sciences, Beijing 100049, China
[c] CSIRO Energy, Private Bag 10, Clayton South, VIC 3169, Australia
[d] School of Mechanical and Chemical Engineering, The University of Western Australia, 35 Stirling Highway, WA 6009, Australia
[e] Key Laboratory of Ministry of Education on Safe Mining of Deep Metal Mines, Northeastern University, Shenyang 110004, China

ARTICLE INFO

Keywords:
Shale gas
Microscopic X-ray computed tomography
Proppant
Permeability anisotropy
Compressibility

ABSTRACT

Hydraulic fracturing is key for shale gas production and fracture permeability or conductivity is one of the most important parameters for gas production rate. Investigating the proppant distribution and fracture permeability in the field is difficult, therefore, laboratory study is a good alternative. In this work, the effect of the layer number and type of proppant on fracture permeability and compressibility were investigated. A cubic shale sample from the Cambrian Niutitang Formation at Sangzhi, Hunan Province, China, was used in this work. Sands and glass beads of different number of layers were added into an artificial fracture and seven cases, including original sample, non-propped fracture, and four kinds of propped fractures were considered. Permeability at three gas pressure steps and five confining pressure steps were measured in each case at two flow directions. Microscopic X-ray computed tomography was used to detect the distributions of proppant, and the relationship with permeability and its anisotropy was studied. A permeability model combining the stress and Klinkenberg effects was used to match experimental data and a new fracture compressibility model was proposed to predict the change of fracture compressibility with the layer number of proppant. It was found that permeability and compressibility of proppant supported fracture are closely related to proppant packing pattern and layer number, as well as the permeability anisotropy. These results improve our understanding on permeability behaviour for the proppant supported fracture and can assist in the model of fracture permeability and simulation of shale gas production.

1. Introduction

Shale gas has become an important natural gas resource in recent years. Production of shale gas increased drastically in the past decade in the U.S. and reached 15.2 Tcf (0.43 Trillion m^3) in 2015, about 50% of total U.S. dry natural gas production [1,2] and triggered significant interest worldwide [3,4]. As shales have very low porosity and permeability, the success of shale gas development owe significantly to the multi-staged hydraulic fracturing technology in horizontal wells [5]. Fracture will dynamically extend in length and aperture to form complex fracture network under the process of multi-staged hydraulic fracturing [6,7]. Moreover, the economic development of shale gas requires not only the large-sale complex fracture system in the reservoir, but also the increased and sustained fracture conductivity [8]. The fracture conductivity, defined as the product of permeability and fracture aperture, is a key indicator to evaluate the effectiveness of fracturing [9]. During hydraulic fracturing, proppant particles are mixed with fracturing fluids and then injected into fracture system to prevent fracture closure, hold fractures open, and obtain high fracture conductivity [10]. Shale fracture conductivity plays a critical role in determining the long term production of shale wells, so studies on the impact of proppant on the fracture conductivity are highly desirable.

Laboratory measurements on propped-fracture conductivity are important for analysing reliable well performance and optimizing fracturing design [11]. The fracture conductivity is affected by rock strength [12], stress [13], the proppant material, size, added amount, distribution and embedment, etc. [10,14–16]. Experimental studies on conductivity for proppant supported fracture of rock cores have been performed [16–18], demonstrating that the permeability of propped sample was drastically improved from the original sample. The effect of proppant embedment on the fracture conductivity on rock cores propped with two types of proppants at different concentrations was

* Corresponding author.
E-mail address: Zhejun.Pan@csiro.au (Z. Pan).

https://doi.org/10.1016/j.fuel.2018.02.141
Received 22 August 2017; Received in revised form 19 February 2018; Accepted 21 February 2018
Available online 27 February 2018

Table 1
TOC content and mineralogical composition of the shale sample.

TOC	Quartz	Feldspar	Calcite	Dolomite	Pyrite	Clay minerals			
						Illite/Smectite	Illite	Chlorite	Chlorite/Smectite
2.4%	42.3%	11.6%	–	–	1.5%	29.9%	7.6%	4.7%	–

studied by Wen et al. [16]. Their results showed that the proppants were not obviously damaged until the closure pressure reached a certain value, and the conductivity was increased by several times when proppant concentration was double. Fredd et al. [17] experimentally studied hydraulic fracture conductivity of fractured sandstone cores, using Jordan sand and sintered bauxite proppants at different concentrations and various closure stresses. The results showed that conductivity could be proppant or asperity dominated depending on the proppant concentration, proppant strength, and formation properties, and the conductivity varied by several orders of magnitude when low strength proppants were used at low concentrations.

Recently, the propped fracture conductivity measurements on shale samples have been performed. For instance, Hou et al. [10] performed measurements on a steel plate, a shale and a sandstone, using three types of proppants to investigate brine conductivity of fracture propped with heterogeneous and uniform proppant placements. Their results indicated that heterogeneous proppant placement led to higher fracture conductivity than a uniform proppant distribution at low closure pressures, and the fracture conductivity was directly proportional to the proppant concentration. Zhang et al. [11] conducted shale conductivity experiments on natural and induced, non-propped and propped fractures. Their results indicated that the larger proppant size and higher concentration led to higher fracture conductivity at elevated closure stress, and proppant partial monolayer failed to maintain the fracture conductivity at elevated closure stresses. Through a series of tests on fractured shale propped with Ottawa sand and ceramic proppants, Kassis and Sondergeld [19] found that a sparse one layer of proppant was equally or more effective than a fairway distribution of proppant in enhancing fracture permeability for both types of proppant, and permeability using sand tended to be higher. However, no studies considered directional fracture permeability or conductivity and the impact of proppant on fracture compressibility.

In order to investigate the directional shale permeability and compressibility of propped fracture, Tan et al. [14] conducted measurements on a shale sample in four different cases. Their results also suggested that adding proppants could significantly increase the absolute permeability but would not signficantly change the fracture compressibility. However, the effect of the layer number and material of proppant on fracture conductivity and fracture compressibility were not studied. Furthermore, they found that proppants could change the direction and ratio of permeability anisotropy, although the directional permeability or conductivity for proppant supported fracture of shale still require further experimental study, especially with better description of proppant distribution in the fracture.

Modelling work on non-propped fracture has been conducted in the past [12,20]. Recently, a few theoretical models have been proposed to estimate the conductivity of propped fracture. Hou et al. [10] developed analytical models to predict the fracture conductivity with a heterogeneous proppant placement. Bortolan Neto et al. [21] developed a simple mathematical model to evaluate the effects of proppant compressibility and in-situ stresses on the hydraulic fracture conductivity. Zhang et al. [22] presented a new correlation to calculate shale fracture conductivity considering proppant properties which could predict the crushed proppant size distribution at increasing closure stress. Khanna et al. [23] proposed a simplified approach to determine the conductivity of narrow fracture propped with a sparse monolayer of proppants, which could provide rough estimates of the optimum proppant concentration. However, these above models did not consider the impact of layer number of proppant on fracture conductivity. Thus, there is a further need to study permeability or conductivity, and compressibility change with respect to effective stress for fracture supported with proppant, as this information is important in understanding and predicting the gas production behaviour from shale reservoirs.

This work studied the effect of different proppant material, size, amount, and distribution on shale fracture permeability and compressibility. Seven different experimental cases were studied on a cubic shale sample from Cambrian Niutitang Formation at Sangzhi, Hunan Province, China. Permeabilities at two different directions along the fracture were measured at three gas pressure steps and five confining pressure steps using methane. After permeability measurement of each proppant supported fracture case, the distribution of proppant was scanned using microscopic X-ray computed tomography (X-ray μ-CT), aiming to investigate the impact of proppant on the change of permeability and its anisotropy in different cases. At last, fracture compressibility in relation to proppant was studied.

2. Experimental

In this study, a shale block was collected from the outcrop of Cambrian Niutitang Formation at Sangzhi, Hunan Province, China. The total organic content (TOC) and mineral composition are shown in Table 1. A cubic sample with a length of 20 mm of each side was cut from the shale block using a wire saw for permeability study. The detailed description of cubic sample cutting can be found in our previous paper [24]. After permeability measurements on the original shale cubic sample, the cubic sample was cut into two pieces along its bedding plane using the wire saw. The cutting simulated a fracture to study the permeability behaviour with proppant.

Glass beads and sands were added to support fracture in two separate configurations: one layer and multiple layers in the fracture. Glass beads are uniform sphere with 0.539 mm in diameter. Sand particles have irregular size and shape, and the range of the length of long axis for sand grains in our experiments is about from 0.43 mm to 1.07 mm. Small amount of water was mixed with the glass beads or sands, making it paste-like and easy to be added between the two pieces of shale. The sample with proppant was wrapped with filter paper and then held in a 3D printed membrane. A standard rubber sleeve was used to hold the cubic sample and the 3D printed membrane before installed in a tri-axial cell. The details about cubic sample installation can be found in Pan et al. [25]. The sample was then put on vacuum for two days to fully remove the water mixed with the proppant before performing permeability measurements.

For the purpose of comparing the impact of proppant on permeability, seven different cases were considered. Before adding proppant in each case, the sample was heated in a vacuumed oven for more than 2 days to dry. The experimental cases are listed as follows:

1. Case 1: original sample.
2. Case 2: the fracture without proppant.
3. Case 3: the fracture propped with one layer of glass beads.
4. Case 4: the fracture propped with multiple layers of glass beads.
5. Case 5: the fracture propped with one layer of sands.
6. Case 6: the fracture propped with multiple layers of sands.

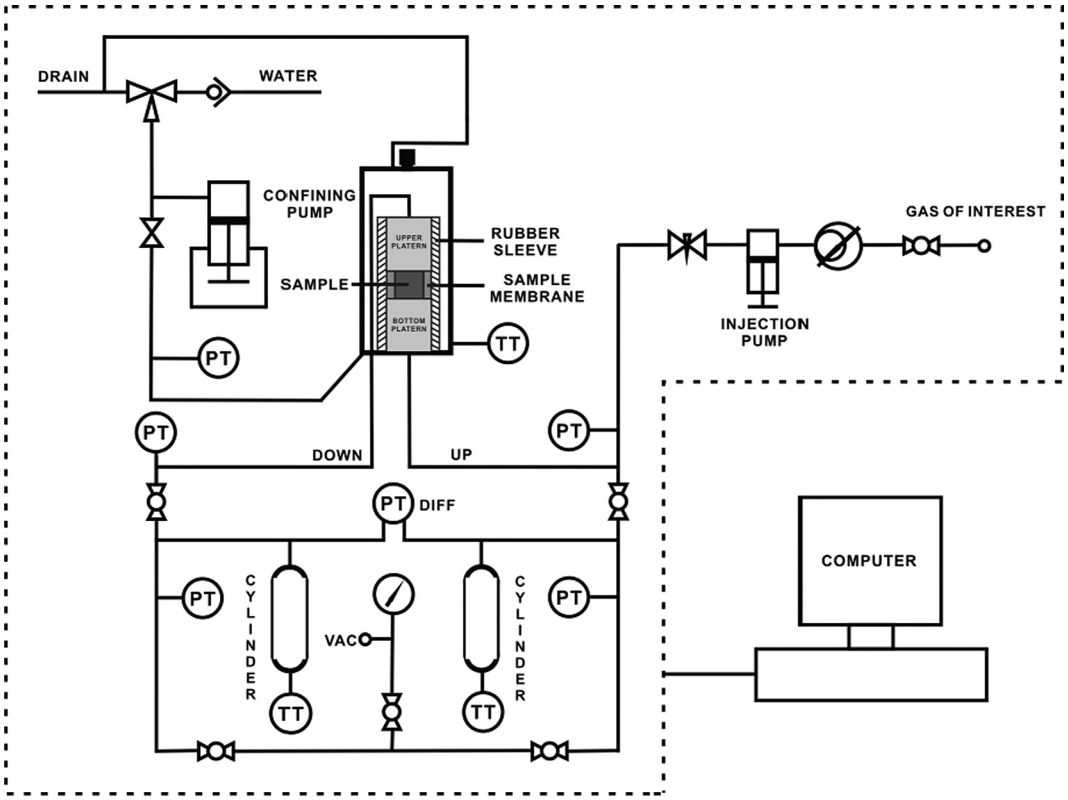

Fig. 1. Experimental instruments (from [25]).

7. Case 7: the fracture after removing proppant.

Permeabilities at three gas pressure steps and five confining pressure steps at each gas pressure were performed in each above case to study the effect of gas pressure and effective stress on permeability. Permeability was measured at two horizontal directions along the fracture in each case. All permeability measurements were conducted at 34.5 °C using methane.

The transient method of Brace et al. [26] was used in this work. This method was widely applied in measuring permeability in reservoir rocks including coal and shale [27,28]. A detailed description of the permeability measurement methods can also be found in Sander et al. [29]. The schematic of the apparatus is shown in Fig. 1. During permeability measurement, gas flows from the upstream gas cylinder to the downstream gas cylinder via the sample. The pressure difference was measured by a differential pressure transducer and permeability can be calculated by [29,30]:

$$\frac{(P_u - P_d)}{(P_{u,0} - P_{d,0})} = e^{-\alpha t} \tag{1}$$

where $P_u - P_d$ and $P_{u,o} - P_{d,o}$ are the differential pressure measured at time t and initial time, respectively. α is defined as below [25,30]:

$$\alpha = \frac{kA(P_{u,0} + P_{d,0})}{2\mu L}\left(\frac{1}{V_u} + \frac{1}{V_d}\right) \tag{2}$$

where k is permeability, A is the cross-sectional area of the cubic sample, L is the length of the cubic sample, and V_u and V_d are the volumes of the upstream and downstream cylinders, respectively [25].

After permeability measurement in each case, the sample with the 3D printed membrane and the sleeve were taken to the Zeiss Xradia XRM520 versa microscopic X-ray computed tomography (X-ray μ-CT) at the Department of Civil Engineering of Monash University for scanning. A resolution of 38 μm was used for scanning the sample. Drishti software was then used to reconstruct the 3D image and to depict the proppant distribution.

3. Results

For each case, the permeability for each horizontal direction at three gas pressures and five confining pressures at each gas pressure was measured. In each case, two to three cycles of permeability measurements at each direction were conducted to examine repeatability. To simplify the comparison, the permeability results measured at the last cycle were presented in corresponding tables and figures below. To study the relationship between fracture permeability and stress, fracture compressibility was calculated using the data for the conditions at almost constant gas pressure and increasing confining pressure. The fracture compressibility can be obtained by fitting permeability with effective stress, using [31]:

$$k = k_0 e^{-3C_f(\sigma - \sigma_0)} \tag{3}$$

where k is the permeability at effective stress σ, k_0 is the permeability at initial effective stress σ_0, and C_f is fracture compressibility. As permeability decreases exponentially with respect to effective stress as shown in Eq. (3), the y axes in Figs. 2–8 are all in logarithmic scale.

3.1. Permeability results: Case 1 – original sample

The first serial permeability measurements were conducted on the original cubic sample before the artificial fracture was cut. The experimental results are listed in Table 2 and plotted in Fig. 2. It can be seen from the results that the permeability is from 6.98×10^{-5} to 4.02×10^{-4} md for gas pressure up to 2.59 MPa and effective stress up to 6.49 MPa. Effective stress (P_e) is defined as the difference between confining pressure (P_c) and gas pressure (P_p). The permeability shows anisotropy with horizontal direction 1 about twice that in horizontal direction 2 at similar pore pressure and effective stress. It also shows that permeability decreases with respect to gas pressure and effective stress. These trends are similar to those in our pervious experimental

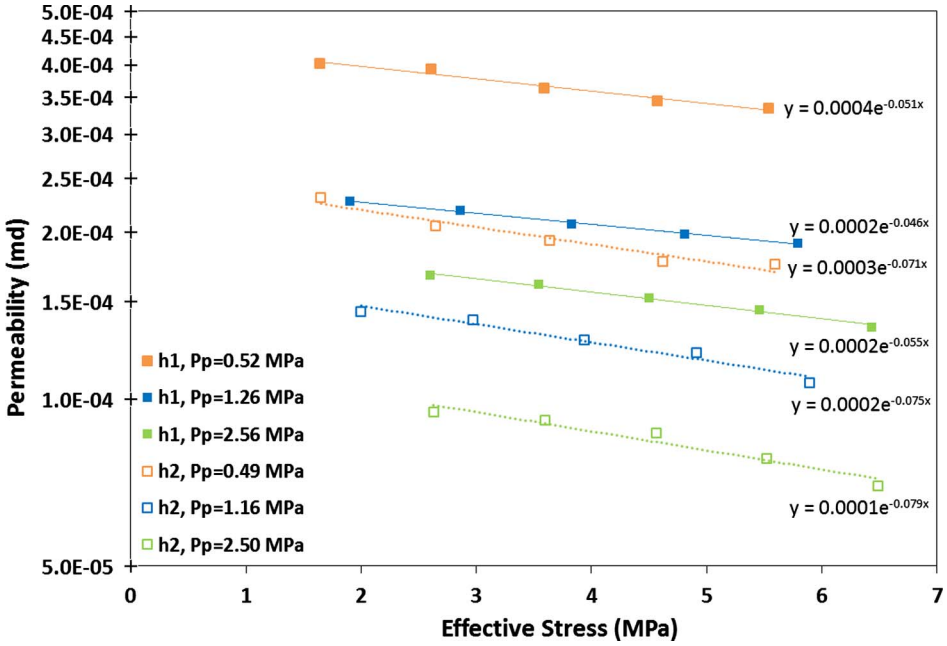

Fig. 2. The permeability results of Case 1 – original sample (solid symbols: horizontal direction 1, empty symbols: horizontal direction 2).

work [14].

3.2. Permeability results: Case 2 – the fracture without proppant

After obtaining the artificial fracture by cutting the cubic sample into two pieces, they were put together for the second serial experimental measurements. The permeability results are presented in Table 3 and plotted in Fig. 3. The permeability is in the range of 0.44–8.02 md, which is thousands times larger than that in Case 1. This suggests that the faces of the artificial fracture were not matched after cutting using the wire saw. However, they are 1 to 2 orders of magnitude lower than the permeability for the fracture supported with proppants, as will be shown in the later sections. On the contrary to Case 1, the permeability in horizontal direction 2 is 4.4–6.6 times that in horizontal direction 1. The ratio of anisotropy is larger than Case 1. The permeability also declines with effective stress and gas pressure (Fig. 3).

3.3. Permeability results: Case 3 – the fracture propped with one layer of glass beads

The permeability is from 19.4 to 30.2 md for this case with one layer of glass beads as shown in Table 4 and Fig. 4. Due to the existence of one layer of glass beads, the permeability is about 16.8–65.8 times and 3.2–8.1 times that of Case 2 in horizontal directions 1 and 2, respectively. Moreover, the ratio of permeability anisotropy after adding one layer of glass beads is 1.2–1.4 at different gas pressures and effective stresses. This shows that adding proppant can increase permeability quite significantly but decrease anisotropy ratio. As shown in Fig. 4, the permeability decreases with respect to effective stress, however,

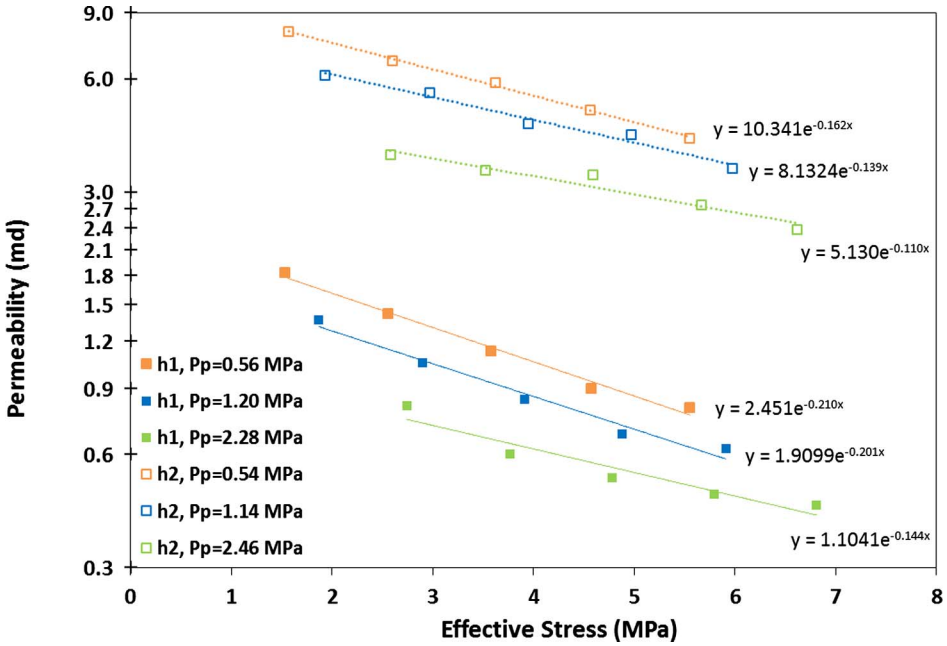

Fig. 3. The permeability results of Case 2 – the fracture without proppant (solid symbols: horizontal direction 1, empty symbols: horizontal direction 2).

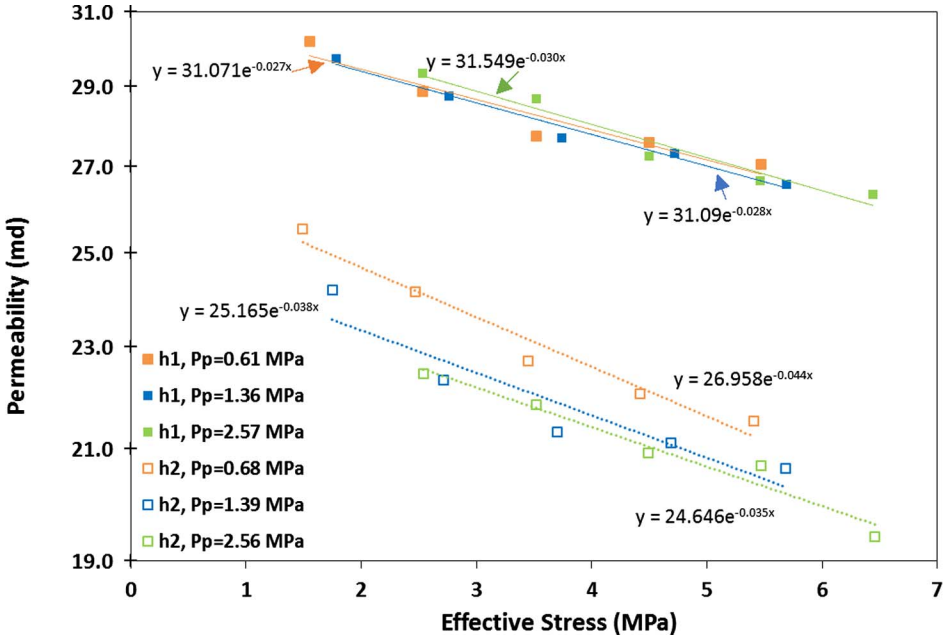

Fig. 4. The permeability results of Case 3 – the fracture propped with one layer of glass beads (solid symbols: horizontal direction 1, empty symbols: horizontal direction 2).

permeability change with gas pressure is less significant in this case.

In addition, fracture conductivity, which is the product of permeability and fracture opening, is also calculated. Fracture opening was obtained from the X-ray μ-CT images. Fracture conductivity of each case with proppant are included in Table 4–7.

3.4. Permeability results: Case 4 – the fracture propped with multiple layers of glass beads

As listed in Table 5 and plotted in Fig. 5, the permeability ranges from 55.1 to 120.4 md for fracture supported with multiple layers of glass beads. After adding multiple layers of glass beads, the permeability is 2.9–4.3 times and 2.7–3.1 times that of in Case 3 in horizontal directions 1 and 2, respectively. The anisotropy ratio of permeability after adding multiple layers of glass beads is 1.4–1.8 which is slightly higher than Case 3 but smaller than that for Cases 1 and 2.

In Case 4, the permeability in horizontal direction 1 slightly decreases with effective stress at a given pore pressure, and decreases more obviously with pore pressure at the similar effective stress. The permeability in horizontal direction 2 obviously decreases with effective stress as well as pore pressure.

3.5. Permeability results: Case 5 – the fracture propped with one layer of sands

The experimental results for Case 5 are presented in Table 6 and Fig. 6. The range of the permeability is from 30.3 to 47.8 md. The permeability of one layer of sands propped fracture is 1.1–1.3 times and 1.6–2.1 times that of Case 3 (one layer of glass beads) in horizontal directions 1 and 2, respectively. In addition, the permeability in

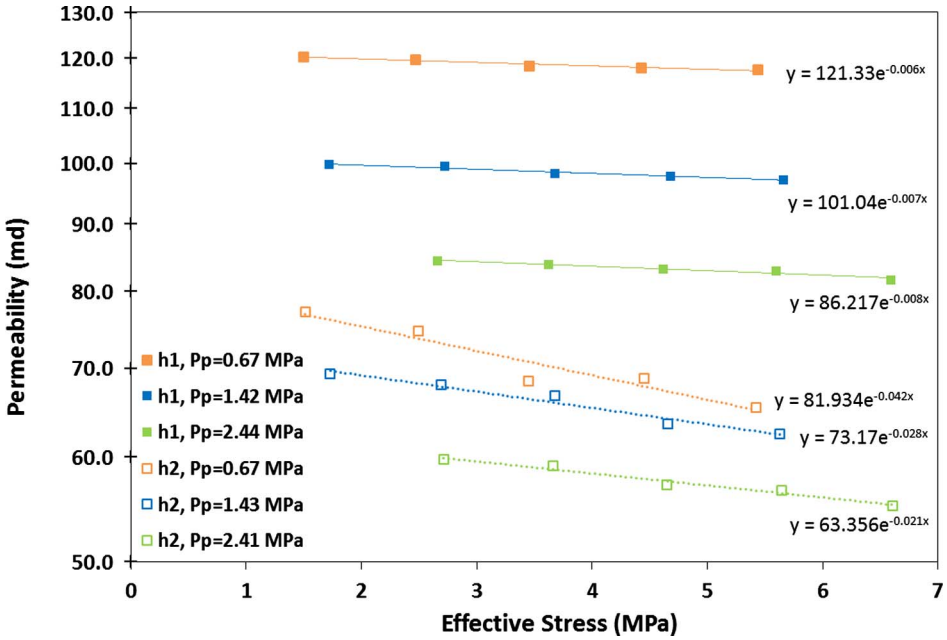

Fig. 5. The permeability results of Case 4 – the fracture propped with multiple layers of glass beads (solid symbols: horizontal direction 1, empty symbols: horizontal direction 2).

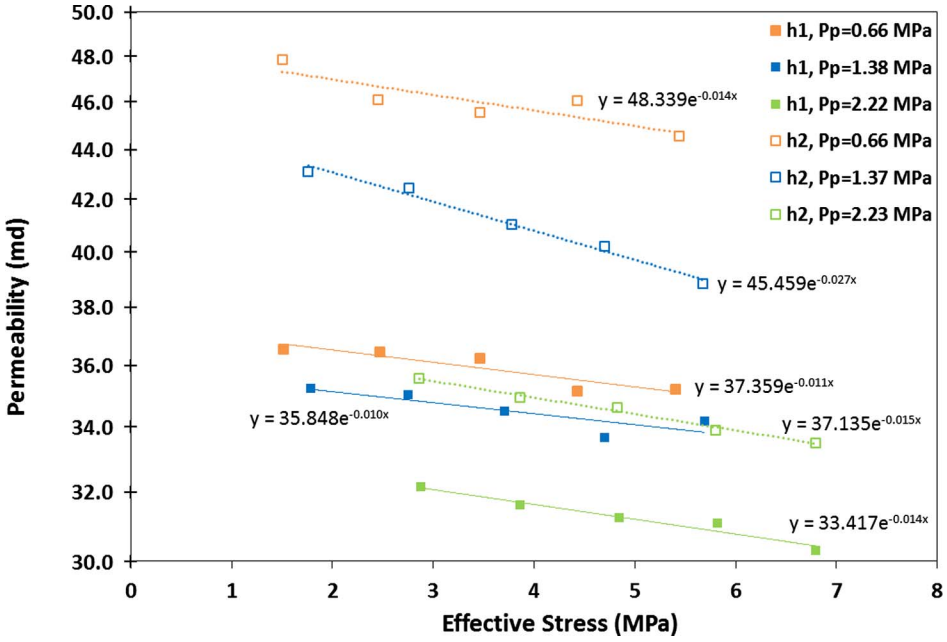

Fig. 6. The permeability results of Case 5 – the fracture propped with one layer of sands (solid symbols: horizontal direction 1, empty symbols: horizontal direction 2).

horizontal direction 2 is 1.1–1.3 times that in horizontal direction 1, which is similar to Case 3.

The permeability has more obvious decreasing trend with effective stress and pore pressure in horizontal direction 2 than in horizontal direction 1.

3.6. Permeability results: Case 6 – the fracture propped with multiple layers of sands

Table 7 and Fig. 7 show the permeability results of fracture propped with multiple layers of sands. The permeability of this case varies from 94.0 to 208.1 md. The permeability of this case is 3.1–4.2 times and 3.7–4.0 times that of Case 5 (one layer of sands) in horizontal directions 1 and 2, respectively; and is 1.2–1.3 times and 2.7–2.9 times that of Case 4 (multiple layers of glass beads) in horizontal directions 1 and 2, respectively. The permeability in horizontal direction 2 is higher than that in horizontal direction1 and the anisotropy ratio is 1.3–1.5. Similar to the comparison of anisotropy ratio between one layer of sands propped fracture and one layer of glass beads propped fracture, the anisotropy ratio of permeability of multiple layers of sands propped fracture slightly also lower than that of multiple layers of glass beads propped fracture. Like all other cases, permeability decreases with effective stress and pore pressure in two horizontal directions.

3.7. Permeability results: Case 7 – the fracture after removing proppant

After completing the permeability measurements for proppant supported fracture, permeability for the non-propped fracture was repeated. The permeability results range from 0.39 to 3.78 md, shown in Table 8 and plotted in Fig. 8. Similar to Case 2, the permeability in

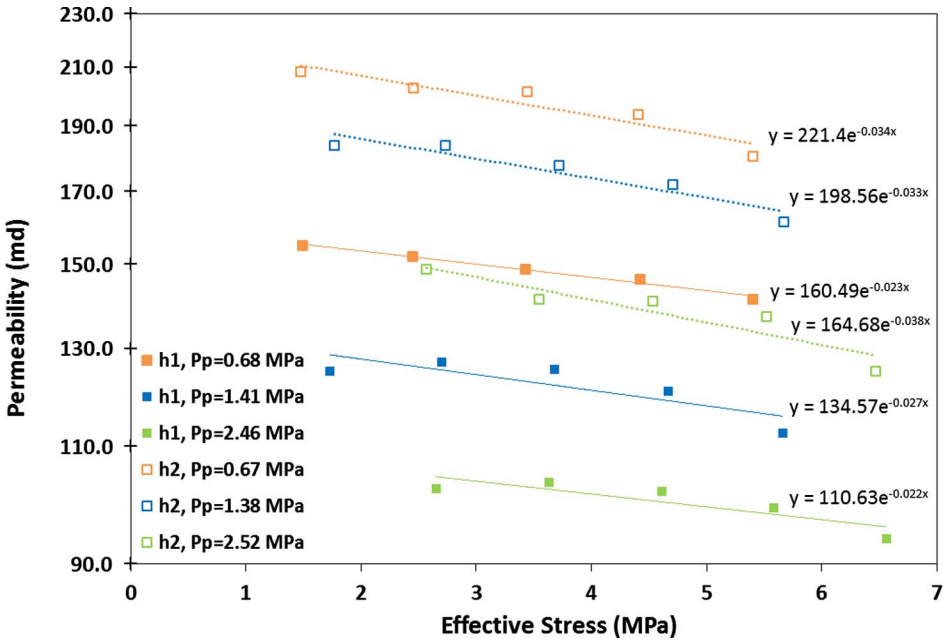

Fig. 7. The permeability results of Case 6 – the fracture propped with multiple layers of sands (solid symbols: horizontal direction 1, empty symbols: horizontal direction 2).

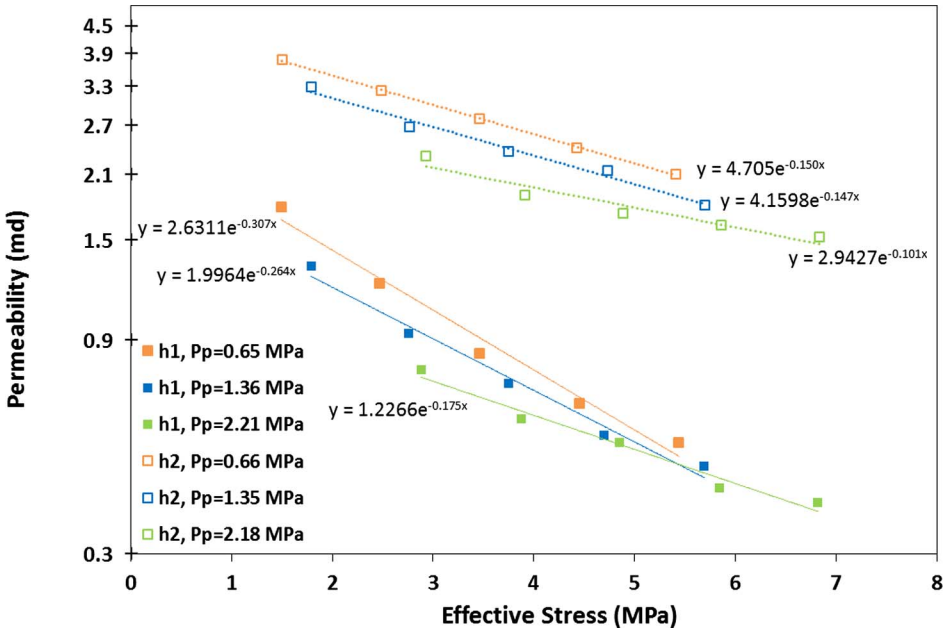

Fig. 8. The permeability results of Case 7 – the fracture after removing proppant (solid symbols: horizontal direction 1, empty symbols: horizontal direction 2).

horizontal direction 2 is higher than that in horizontal direction 1, although the anisotropic ratio of permeability is slightly lower than that in Case 2. However, the permeability between Case 2 and this case show difference, suggesting that recombining the two pieces of the shale may not achieve the same results. Nevertheless, the difference in permeability is small enough compared to those of proppant supported fracture.

4. Discussion

4.1. Permeability and proppant distribution

The permeability results of the original sample (Case 1) are in the range of literature results, which are around hundred nanodarcy [27,32]. Tan et al. [14] showed that permeability of a natural non-propped fracture had almost no improvement to the original sample. In this work, an artificial fracture was cut using a wire saw to simulate a flat surface of the fracture so that different amount of proppant can be added. Although the permeability of the non-propped fracture (Case 2 and Case 7) is relatively high, but once supported with high-strength proppant, the permeability become proppant dominated [17] and this is shown in this work too.

The distributions of proppant in the four cases, Cases 3–6, were scanned by X-ray μ-CT and the 3D reconstructed images are shown in Figs. 9–12, respectively. From these reconstructed images, it can be seen that the proppant particles were closely packed, except for Case 5, in which one layer of sands was added in the fracture. This was because that not enough sands were added.

As shown in the Results section, the permeability descending order among the four cases with proppant are: multiple layers of sands, multiple layers of glass beads, one layer of sands, and one layer of glass beads. In this work, it shows that irregular shaped sands (Cases 5 and 6) are more effective than sphere shaped glass beads (Cases 3 and 4) in improving fracture permeability or conductivity. This can be seen from the images depicting the void for each case in Figs. 9–12, where the green colour shows the void volume and they are less in glass beads cases (Cases 3 and 4) than those in sands cases (Cases 5 and 6). One reason is that more irregular in shape particles are more difficult to form closely packed pattern, leaving larger gaps between non-touching surfaces and leading to greater porosity [33], thus permeability. It can be seen from Figs. 9 and 10, the more regular shaped glass beads are closer to densely packed pattern, which usually have smaller porosity.

Table 2
The permeability results of Case 1 – original sample.

Horizontal direction 1				Horizontal direction 2			
P_p (MPa)	P_c (MPa)	P_e (MPa)	k (md)	P_p (MPa)	P_c (MPa)	P_e (MPa)	k (md)
0.51	2.15	1.64	4.02×10^{-4}	0.51	2.15	1.65	2.31×10^{-4}
0.52	3.13	2.61	3.93×10^{-4}	0.49	3.13	2.65	2.05×10^{-4}
0.53	4.11	3.59	3.63×10^{-4}	0.48	4.12	3.64	1.93×10^{-4}
0.53	5.09	4.57	3.45×10^{-4}	0.49	5.10	4.62	1.77×10^{-4}
0.53	6.07	5.54	3.34×10^{-4}	0.49	6.08	5.59	1.75×10^{-4}
1.23	3.13	1.90	2.27×10^{-4}	1.14	3.14	2.00	1.44×10^{-4}
1.25	4.11	2.86	2.19×10^{-4}	1.15	4.12	2.97	1.39×10^{-4}
1.26	5.09	3.83	2.07×10^{-4}	1.16	5.10	3.94	1.28×10^{-4}
1.27	6.07	4.81	1.98×10^{-4}	1.17	6.08	4.91	1.21×10^{-4}
1.27	7.06	5.79	1.91×10^{-4}	1.17	7.06	5.89	1.07×10^{-4}
2.50	5.10	2.60	1.67×10^{-4}	2.47	5.10	2.63	9.46×10^{-5}
2.54	6.08	3.54	1.61×10^{-4}	2.48	6.08	3.60	9.15×10^{-5}
2.56	7.06	4.50	1.52×10^{-4}	2.50	7.06	4.56	8.69×10^{-5}
2.58	8.04	5.46	1.45×10^{-4}	2.52	8.04	5.52	7.82×10^{-5}
2.59	9.01	6.43	1.35×10^{-4}	2.53	9.02	6.49	6.98×10^{-5}

Table 3
The permeability results of Case 2 – the fracture without proppant.

Horizontal direction 1				Horizontal direction 2			
P_p (MPa)	P_c (MPa)	P_e (MPa)	k (md)	P_p (MPa)	P_c (MPa)	P_e (MPa)	k (md)
0.62	2.14	1.53	1.83	0.58	2.15	1.57	8.02
0.59	3.13	2.55	1.42	0.54	3.14	2.60	6.69
0.54	4.11	3.58	1.13	0.50	4.12	3.62	5.86
0.53	5.10	4.57	0.90	0.54	5.09	4.56	4.95
0.52	6.07	5.55	0.80	0.52	6.07	5.55	4.17
1.24	3.12	1.87	1.37	1.20	3.13	1.93	6.13
1.21	4.11	2.90	1.05	1.14	4.11	2.97	5.52
1.20	5.11	3.91	0.84	1.15	5.10	3.95	4.55
1.19	6.06	4.88	0.68	1.10	6.07	4.97	4.26
1.15	7.06	5.91	0.62	1.09	7.05	5.97	3.46
2.36	5.09	2.74	0.81	2.51	5.10	2.58	3.76
2.31	6.08	3.77	0.60	2.56	6.08	3.52	3.43
2.28	7.06	4.78	0.52	2.47	7.06	4.59	3.32
2.25	8.04	5.79	0.47	2.37	8.04	5.67	2.77
2.20	9.01	6.81	0.44	2.40	9.01	6.62	2.38

Moreover, the sand particles are larger (up to more than 1 mm) in size than the glass beads (~0.54 mm) used in this work, leaving void space volume between particles even larger. Larger void space (or the pore volume) between the proppant particles will also leads to high permeability because permeability is also related to the pore size.

It should be noted that the case of one layer of sands in this work (Fig. 11) provided the highest porosity in the fracture because the amount of sands was not sufficiently filled in the fracture. However, the permeability is still lower than that with multiple layers of sands, suggesting that adding more layers of proppant is more preferential in improving fracture permeability and thus conductivity. This is consistent with the literature results [34] that adding multiple layers of proppant is an effective means to increase fracture permeability, as multiple layers of proppant causes wider aperture of fracture and more void volume in fracture.

It would be better if porosity of the proppant supported fracture can be quantitatively obtained from the CT results and then compared with permeability in different cases. Although the 3D image processing software is able to calculate the porosity, it depends on the cut-off value used to differentiate void space and proppant. The cut-off value can be arbitrary and different to each CT scan, making porosity comparison among different cases difficult. However, the void space distribution in each case can be well used to investigate its relationship with anisotropic permeability, to be discussed later.

4.2. Permeability and fracture compressibility

Gas permeability in porous rocks, such as shale and coal, is a function of gas pressure and effective stress. Recently, Pan et al. [25] combined the stress and Klinkenberg effects, and used the following model to match their experimental permeability data for shales:

$$k = k_a\left(1 + \frac{b}{P_p}\right)e^{-3C_f(\sigma-\sigma_0)} \tag{4}$$

where k_a is the absolute permeability at initial effective stress σ_0, b is the Klinkenberg constant, P_p is pore pressure and C_f is fracture compressibility. The model has been applied in Tan et al. [14] to describe the permeability for shale natural fracture with and without proppant. The model is applied here to describe the permeability results. The modelling results and the model parameters are listed in Table 9. It can be seen that compressibility for proppant supported fracture is much lower than original sample and the open fracture without proppant meaning that the fracture permeability with proppant is less stress sensitive.

A useful analysis is how fracture compressibility changes with respect to the number of proppant layers in the fracture, as injected proppant will form decreased number of layers in the hydraulic fracture from well to the tip of the fracture. Studying the fracture compressibility is important in understanding how fracture permeability changes. In the modelling work below, both the formation rock and proppant

Table 4
The permeability results of Case 3 – the fracture propped with one layer of glass beads.

Horizontal direction 1					Horizontal direction 2				
P_p (MPa)	P_c (MPa)	P_e (MPa)	k (md)	C (md*m)	P_p (MPa)	P_c (MPa)	P_e (MPa)	k (md)	C (md*m)
0.61	2.15	1.55	30.2	0.020	0.67	2.16	1.49	25.5	0.017
0.61	3.13	2.53	28.9	0.019	0.68	3.14	2.47	24.1	0.016
0.61	4.13	3.52	27.8	0.018	0.68	4.13	3.45	22.7	0.015
0.61	5.10	4.50	27.6	0.018	0.68	5.10	4.42	22.1	0.015
0.61	6.08	5.47	27.1	0.018	0.68	6.09	5.41	21.5	0.014
1.35	3.14	1.78	29.7	0.020	1.39	3.14	1.75	24.2	0.016
1.36	4.12	2.76	28.8	0.019	1.40	4.11	2.71	22.3	0.015
1.37	5.11	3.74	27.7	0.018	1.40	5.10	3.70	21.3	0.014
1.36	6.08	4.72	27.3	0.018	1.38	6.07	4.69	21.1	0.014
1.37	7.06	5.69	26.6	0.018	1.39	7.07	5.68	20.6	0.014
2.56	5.09	2.53	29.3	0.019	2.56	5.10	2.54	22.5	0.015
2.57	6.09	3.52	28.7	0.019	2.56	6.08	3.52	21.8	0.014
2.56	7.06	4.50	27.2	0.018	2.56	7.05	4.49	20.9	0.014
2.57	8.03	5.46	26.7	0.018	2.57	8.04	5.47	20.7	0.014
2.57	9.02	6.44	26.3	0.017	2.57	9.02	6.46	19.4	0.013

Table 5
The permeability results of Case 4 – the fracture propped with multiple layers of glass beads.

Horizontal direction 1					Horizontal direction 2				
P_p (MPa)	P_c (MPa)	P_e (MPa)	k (md)	C (md*m)	P_p (MPa)	P_c (MPa)	P_e (MPa)	k (md)	C (md*m)
0.66	2.16	1.50	120.4	0.17	0.66	2.17	1.51	77.1	0.11
0.67	3.13	2.47	119.8	0.17	0.67	3.17	2.49	74.7	0.11
0.66	4.12	3.46	118.3	0.17	0.67	4.12	3.45	68.4	0.10
0.67	5.10	4.43	118.0	0.17	0.67	5.12	4.45	68.7	0.10
0.67	6.11	5.44	117.7	0.17	0.67	6.08	5.42	65.3	0.10
1.42	3.13	1.72	99.7	0.14	1.43	3.16	1.73	69.3	0.10
1.42	4.14	2.72	99.4	0.14	1.43	4.12	2.69	68.0	0.10
1.41	5.09	3.68	98.2	0.14	1.43	5.10	3.68	66.7	0.10
1.42	6.10	4.68	97.8	0.14	1.42	6.08	4.66	63.5	0.092
1.42	7.08	5.66	97.1	0.14	1.43	7.05	5.63	62.4	0.091
2.45	5.10	2.66	84.4	0.12	2.41	5.12	2.71	59.7	0.087
2.45	6.08	3.62	83.8	0.12	2.42	6.08	3.66	59.1	0.086
2.44	7.06	4.62	83.2	0.12	2.42	7.07	4.65	57.1	0.083
2.44	8.04	5.60	82.9	0.12	2.41	8.05	5.64	56.6	0.082
2.44	9.02	6.59	81.6	0.12	2.41	9.01	6.61	55.1	0.080

Table 6
The permeability results of Case 5 – the fracture propped with one layer of sands.

Horizontal direction 1					Horizontal direction 2				
P_p (MPa)	P_c (MPa)	P_e (MPa)	k (md)	C (md*m)	P_p (MPa)	P_c (MPa)	P_e (MPa)	k (md)	C (md*m)
0.66	2.17	1.51	36.6	0.021	0.66	2.16	1.50	47.8	0.028
0.67	3.13	2.47	36.5	0.021	0.67	3.12	2.45	46.1	0.027
0.66	4.11	3.46	36.2	0.021	0.66	4.12	3.46	45.5	0.027
0.67	5.10	4.43	35.1	0.020	0.66	5.09	4.43	46.0	0.027
0.66	6.06	5.40	35.2	0.021	0.66	6.10	5.44	44.5	0.026
1.37	3.15	1.78	35.2	0.021	1.37	3.13	1.76	43.1	0.025
1.38	4.13	2.75	35.0	0.020	1.37	4.12	2.76	42.5	0.025
1.38	5.08	3.71	34.5	0.020	1.36	5.14	3.78	41.0	0.024
1.38	6.08	4.70	33.7	0.020	1.37	6.07	4.70	40.2	0.023
1.37	7.06	5.69	34.2	0.020	1.37	7.04	5.67	38.8	0.023
2.22	5.11	2.88	32.1	0.019	2.23	5.09	2.86	35.6	0.021
2.22	6.08	3.86	31.6	0.018	2.23	6.09	3.86	34.9	0.020
2.22	7.07	4.84	31.2	0.018	2.23	7.06	4.83	34.6	0.020
2.23	8.05	5.82	31.1	0.018	2.23	8.03	5.80	33.9	0.020
2.22	9.01	6.79	30.3	0.018	2.22	9.01	6.79	33.5	0.020

Table 7
The permeability results of Case 6 – the fracture propped with multiple layers of sands.

Horizontal direction 1					Horizontal direction 2				
P_p (MPa)	P_c (MPa)	P_e (MPa)	k (md)	C (md*m)	P_p (MPa)	P_c (MPa)	P_e (MPa)	k (md)	C (md*m)
0.67	2.16	1.49	154.8	0.83	0.67	2.15	1.48	208.1	1.11
0.68	3.13	2.45	151.9	0.81	0.67	3.13	2.46	202.6	1.09
0.69	4.12	3.43	148.8	0.80	0.66	4.10	3.44	201.4	1.08
0.69	5.11	4.42	146.1	0.78	0.67	5.08	4.41	193.7	1.04
0.68	6.08	5.40	141.4	0.76	0.67	6.07	5.40	180.3	0.97
1.41	3.14	1.73	124.9	0.67	1.38	3.15	1.77	183.7	0.98
1.41	4.11	2.70	127.0	0.68	1.38	4.11	2.73	183.5	0.98
1.42	5.10	3.68	125.4	0.67	1.39	5.11	3.72	177.4	0.95
1.42	6.09	4.67	120.7	0.65	1.38	6.08	4.71	171.9	0.92
1.40	7.06	5.66	112.5	0.60	1.39	7.06	5.67	161.2	0.86
2.45	5.11	2.65	102.3	0.55	2.52	5.10	2.57	148.7	0.80
2.46	6.09	3.63	103.3	0.55	2.53	6.08	3.55	141.2	0.76
2.46	7.07	4.61	101.9	0.55	2.51	7.04	4.53	140.8	0.75
2.46	8.04	5.58	98.9	0.53	2.51	8.03	5.52	137.3	0.74
2.46	9.02	6.56	94.0	0.50	2.53	9.00	6.47	124.9	0.67

packing are considered as linear elastic media. Analysis of fracture compressibility is based on the propped fracture stress–strain behaviour. The fracture compressibility is defined as [28]:

$$C_f = -\frac{1}{\phi}\frac{\partial \phi}{\partial \sigma} \tag{5}$$

where ϕ is porosity of the fracture with proppant.

For the fracture propped with multiple layers of proppants, it can be divided into two regions, shown in Fig. 13: (1) half of the layer close to the rock on each side of the fracture, where compressibility is impacted by both the rock and proppant; its pore volume to the total fracture volume is ϕ_1; (2) $n-1$ layers of middle zone, where compressibility is

Table 8
The permeability results of Case 7 – the fracture after removing proppant.

Horizontal direction 1				Horizontal direction 2			
P_p (MPa)	P_c (MPa)	P_e (MPa)	k (md)	P_p (MPa)	P_c (MPa)	P_e (MPa)	k (md)
0.66	2.15	1.49	1.78	0.66	2.17	1.50	3.78
0.66	3.13	2.47	1.20	0.66	3.15	2.49	3.22
0.65	4.11	3.46	0.84	0.66	4.12	3.46	2.79
0.65	5.10	4.45	0.65	0.66	5.10	4.43	2.41
0.65	6.09	5.44	0.53	0.67	6.07	5.41	2.10
1.36	3.15	1.79	1.31	1.35	3.15	1.79	3.28
1.36	4.12	2.76	0.93	1.35	4.12	2.77	2.68
1.36	5.10	3.75	0.72	1.35	5.10	3.75	2.36
1.36	6.06	4.70	0.55	1.35	6.08	4.73	2.14
1.37	7.05	5.69	0.47	1.35	7.05	5.70	1.79
2.22	5.10	2.88	0.77	2.18	5.11	2.93	2.31
2.20	6.08	3.88	0.60	2.17	6.08	3.91	1.89
2.21	7.05	4.85	0.53	2.18	7.07	4.89	1.72
2.20	8.04	5.84	0.42	2.17	8.04	5.86	1.62
2.20	9.02	6.82	0.39	2.18	9.01	6.84	1.52

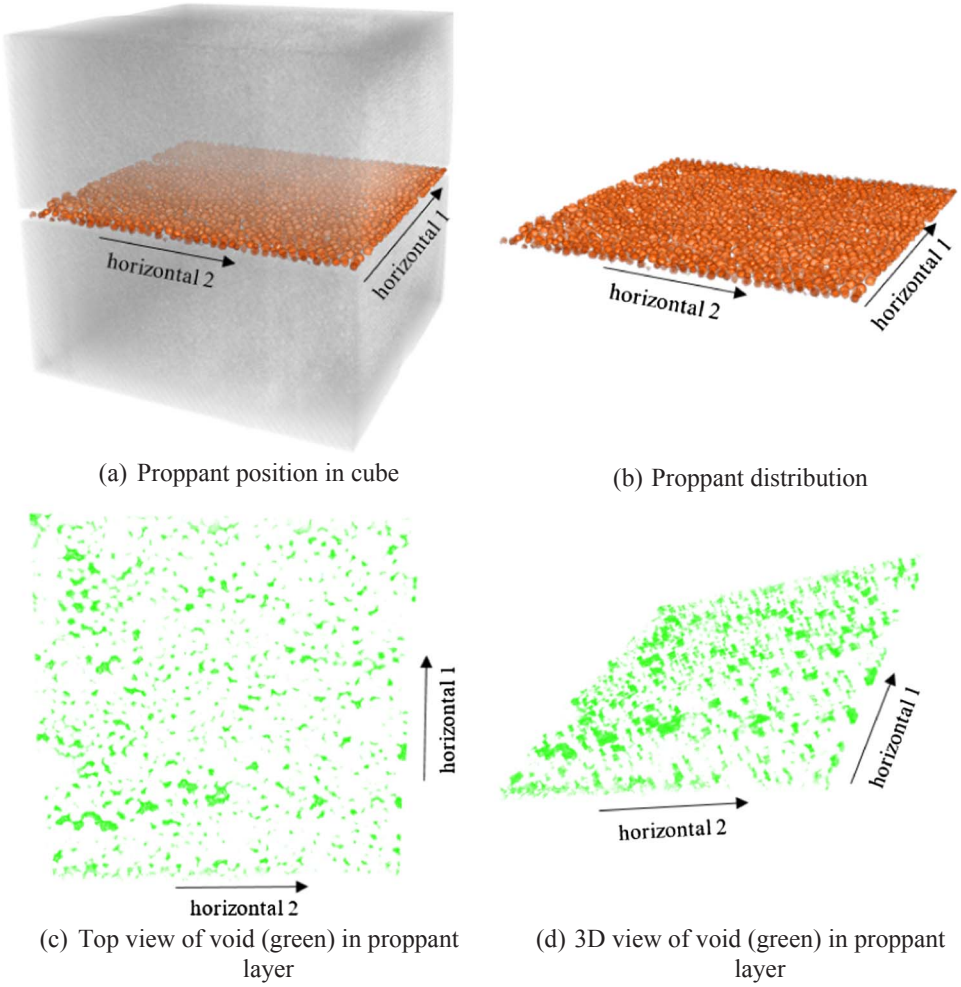

(a) Proppant position in cube (b) Proppant distribution

(c) Top view of void (green) in proppant layer (d) 3D view of void (green) in proppant layer

Fig. 9. The distribution of one layer of glass beads in fracture (Case 3).

only impacted by the proppants; its pore volume to the total fracture volume is ϕ_2. Therefore, the fracture compressibility can be rewritten as:

$$C_f = -\frac{1}{\phi_1 + \phi_2}\frac{\partial(\phi_1 + \phi_2)}{\partial\sigma} \tag{6}$$

It can be converted into:

$$C_f = \frac{\phi_1}{\phi_1 + \phi_2}C_{f1} + \frac{\phi_2}{\phi_1 + \phi_2}C_{f2} \tag{7}$$

where $C_{f1} = -\frac{1}{\phi_1}\frac{\partial\phi_1}{\partial\sigma}$ is compressibility for the pores next to the fracture surface, and $C_{f2} = -\frac{1}{\phi_2}\frac{\partial\phi_2}{\partial\sigma}$ is compressibility of the pores in the proppant only zone in the middle of the fracture.

Particle packing arrangement has its own porosity, for instance the

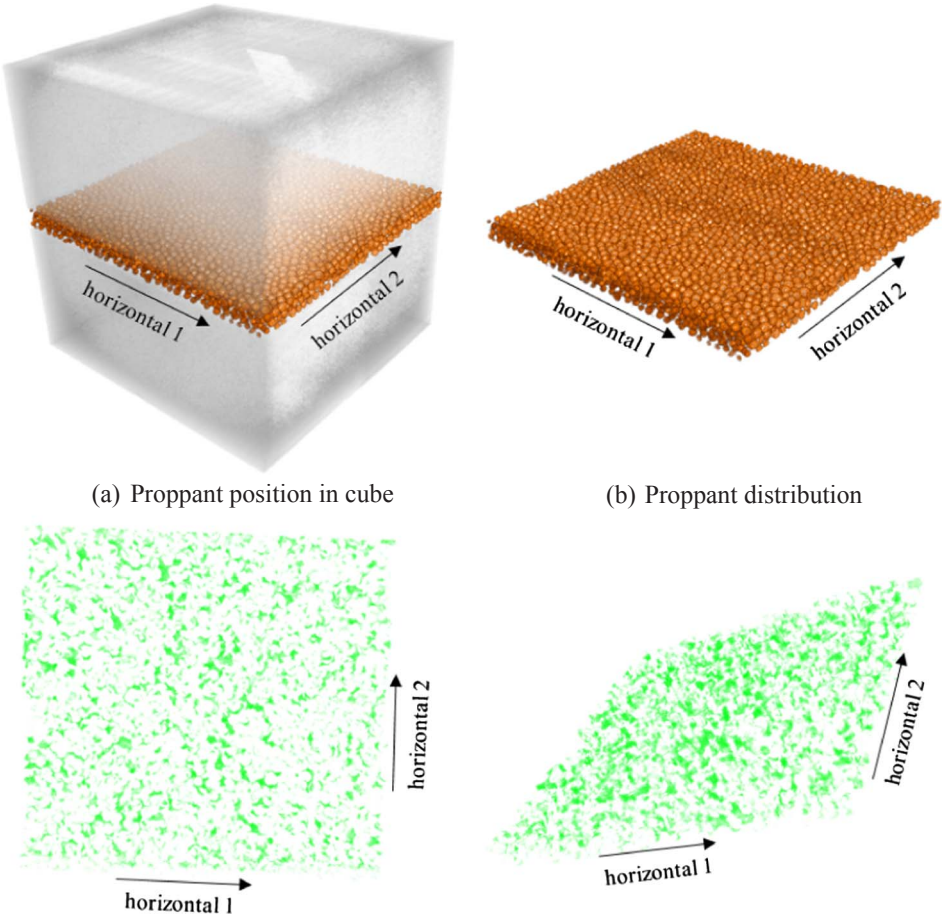

(a) Proppant position in cube (b) Proppant distribution

(c) Top view of void (green) in proppant layer (d) 3D view of void (green) in proppant layer

Fig. 10. The distribution of multiple layers of glass beads in fracture (Case 4).

triclinic packing of spheres has a porosity of about 26.0% and the porosity of the orthorhombic packing is 39.5% [35]. Use ϕ_a and ϕ_b to respectively represent the intrinsic porosity of the different packings in the proppant zone next to the fracture surface and the proppant zone in the middle of the fracture, it yields:

$$\phi_1 = \frac{\phi_a}{n} \text{ and } \phi_2 = \frac{\phi_b(n-1)}{n} \tag{8}$$

Therefore, Eq. (7) can be written as:

$$C_f = \frac{\phi_a}{\phi_a + \phi_b(n-1)} C_{f1} + \frac{\phi_b(n-1)}{\phi_a + \phi_b(n-1)} C_{f2} \tag{9}$$

Therefore, the compressibility of the proppant supported fracture can be described by the number of layers of proppant, the packing porosity which can be obtained by assuming a packing pattern, the compressibilities in the two zones which are related to the mechanical properties of the rock and proppant, and the packing pattern of the proppant. ϕ_a = 39.5% and ϕ_b = 26.0% are used in the modelling work below.

From Figs. 10 and 12, it can be seen that approximate three layers of proppant were added in both Case 4 and Case 6. The compressibility results of C_f of the propped fracture in Table 9 are matched and shown in Fig. 14. The results show that fracture compressibility presents different trends between glass beads and sands propped fracture. For glass beads propped fracture, the compressibility in two horizontal directions both decrease with increasing layer number of proppant exponentially. While for sands propped fracture, the compressibility in two horizontal directions both increase with increasing layer number of proppant.

It should be noted that there are only two data points for each modelling fit and more data points will be more helpful to verify the model. Nevertheless, the model demonstrates the trend that the fracture compressibility will equal to the packed proppant compressibility with the layer number increase. This model is useful in the prediction of fracture permeability or conductivity during reservoir simulation to better represent the permeability in the fracture where the number of proppant layers varies at different locations.

4.3. Permeability anisotropy

For original sample without fracture (Case 1), the permeability in horizontal direction 1 is twice that in horizontal direction 2 at similar pore pressure and effective stress. That is because different horizontal directions have directional pore, fabric and micro fracture distribution [30,36–38].

For fracture without proppant in Case 2, the permeability in horizontal direction 2 is about 4.4–6.6 times that in horizontal direction 1. This ratio is about 2.1–4.2 times in Case 7, in which the fracture was not propped either. The permeability anisotropy became stronger than that in Case 1, suggesting that the fracture faces cut by the wire saw were not smooth. For the cases with proppant (Cases 3–6), the permeability anisotropic ratio is significantly reduced. For fracture with one layer of glass beads (Case 3), the permeability in horizontal direction 1 is 1.2–1.4 times that in horizontal direction 2. It is 1.4–1.8 times in Case 4, in which multiple layers of glass beads were added in the fracture.

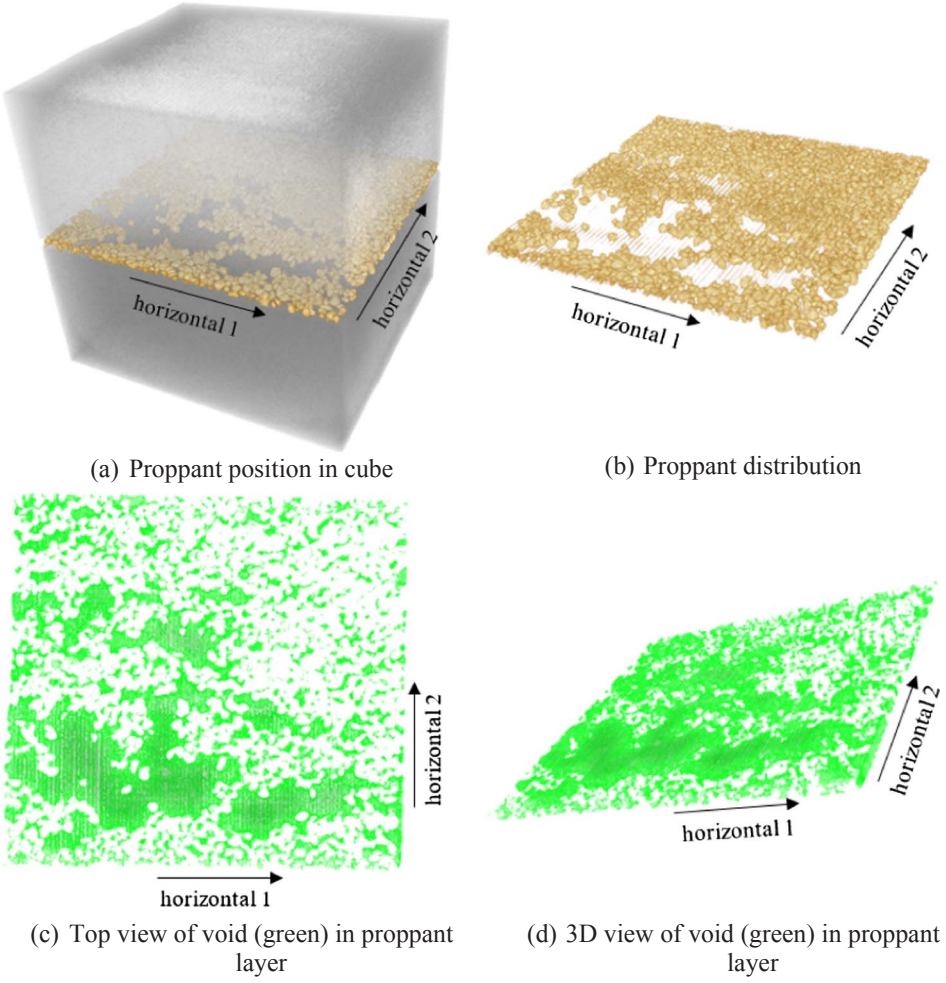

(a) Proppant position in cube (b) Proppant distribution

(c) Top view of void (green) in proppant layer (d) 3D view of void (green) in proppant layer

Fig. 11. The distribution of one layer of sands in fracture (Case 5).

Table 9
Permeability modelling parameters.

Flow direction	Parameter	Case 1	Case 2	Case 3	Case 4	Case 5	Case 6	Case 7
Horizontal direction 1	k_a (md)	1.21×10^{-4}	1.44	31.20	76.33	32.94	97.51	1.80
	C_f (MPa^{-1})	0.014	0.078	0.0093	0.0030	0.0051	0.0083	0.10
	b (MPa)	1.31	0.48	0.00	0.41	0.11	0.46	0.31
	AAD%	1.09	8.54	0.77	2.31	2.09	2.49	9.10
Horizontal direction 2	k_a (md)	8.45×10^{-5}	5.68	24.47	65.43	35.95	154.00	3.40
	C_f (MPa^{-1})	0.025	0.051	0.013	0.012	0.0080	0.013	0.050
	b (MPa)	1.06	0.44	0.056	0.16	0.27	0.32	0.26
	AAD%	4.05	6.49	1.21	2.58	3.35	4.54	4.13

Moreover, the permeability in horizontal direction 2 is 1.1–1.3 times that in horizontal direction 1 for fracture propped with one layer of sands (Case 5). It is 1.3–1.5 times for fracture propped with multiple layers of sands (Case 6). From the above comparison, adding proppant decreased the anisotropy ratio of fracture permeability. It seems to contradict with our previous research [14], in which adding glass beads caused the lager anisotropy ratio of fracture permeability than non-propped fracture. Note that the proppant distribution in Tan et al. [14] was even more uneven because of the topology of the fracture (mainly distribute on the two ends along horizontal direction 1) as well as the smaller amount of proppants than this work. In this paper, the proppants were more densely packed. This work and our previous research [14] studied permeability anisotropy for shale fracture supported with proppant under different conditions, demonstrating that permeability behaviour in proppant supported fractures are complex and factors including fracture topology and proppant shape, size and packing pattern all play important roles.

From Figs. 9–12, it can be seen that the void space distribution are directional, shown as in green. This is in good accordance to the permeability anisotropy ratio analysed above. One exception is Case 5 with single layer of sands shown in Fig. 11. There was more connected void space in horizontal direction 1 than horizontal direction 2, while the permeability anisotropy shows otherwise. Because the sands were not filled in the entire fracture in this case, there was a likelihood that the sands moved their locations. Therefore, the permeability anisotropy and CT results are not in accordance.

5. Conclusions

In this work, we measured shale fracture permeability for seven

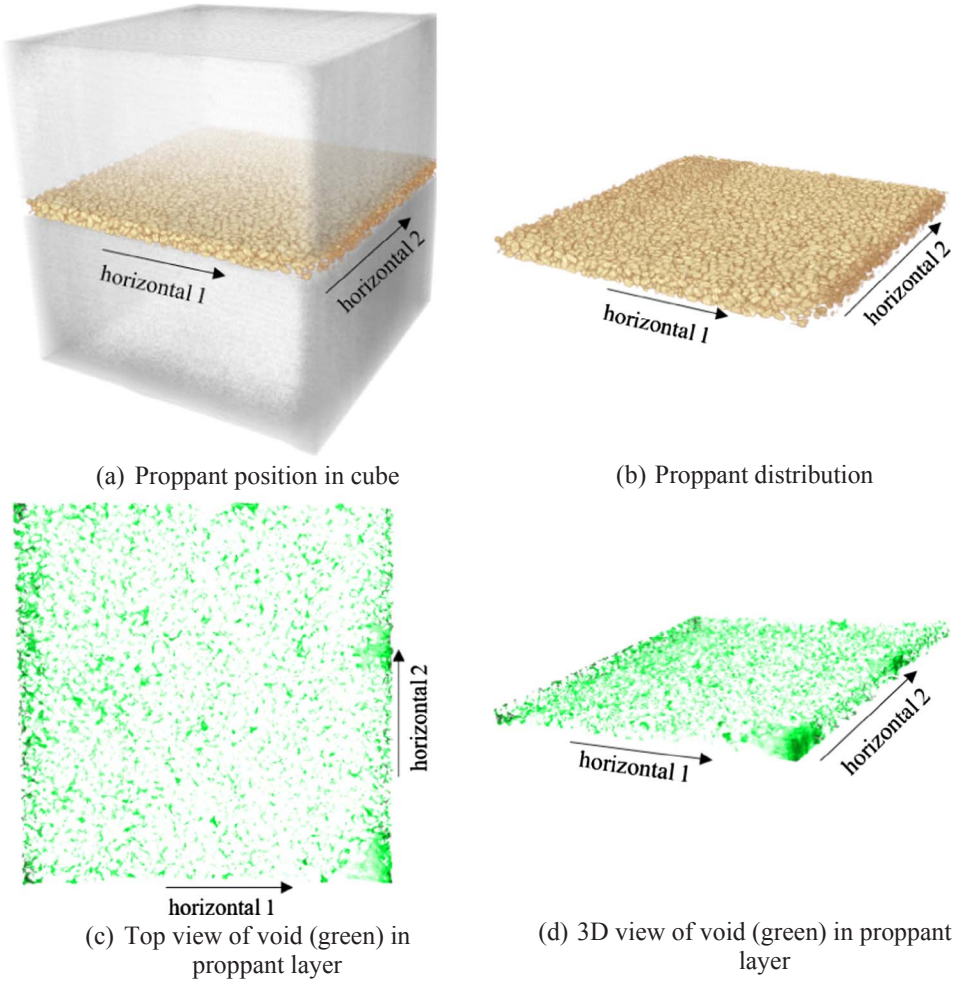

(a) Proppant position in cube (b) Proppant distribution

(c) Top view of void (green) in proppant layer (d) 3D view of void (green) in proppant layer

Fig. 12. The distribution of multiple layers of sands in fracture (Case 6).

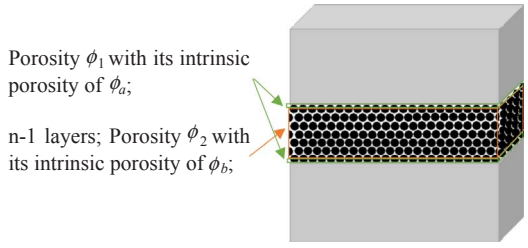

Fig. 13. The schematic diagram of multiple layers of proppant in fracture.

different cases (including no fracture, non-propped fracture and propped fracture with different types and amount of proppant) using methane. The effect of the layer number and type of proppant on fracture permeability and fracture compressibility were investigated. X-ray μ-CT was used to detect the distribution of proppant in the fracture. A permeability model combining the stress and Klinkenberg effects was used to match experimental data. By dividing the propped fracture into two sections, a fracture compressibility model was proposed to predict the fracture compressibility with the number of proppant layers. The following conclusions can be drawn:

1. Fracture permeability is closely related to proppant packing and layer number. In this work, the permeability is in descending order from multiple layers of sands, multiple layers of glass beads, one layer of sands, to one layer of glass beads. Permeability can reach hundreds of millidarcy with 3 layers of proppant with fracture width of 1.5 mm; and the irregular shaped and larger sized sands leave more void volume between particles, resulting to higher permeability.
2. Fracture compressibility decreases for proppant supported fracture, meaning fracture permeability is less sensitive to stress. The fracture compressibility presents different change trends with respect to number of layers for glass beads and sands. For glass beads propped fracture, the compressibility in two horizontal directions both decrease with increasing layer number of proppant exponentially. While for sands propped fracture, the compressibility in two horizontal directions both increase with increasing layer number of proppant exponentially.
3. Adding proppant decreases the anisotropy ratio of the fracture permeability. The permeability anisotropy is more related to the void space distribution between the proppant particles and it is less related to the permeability anisotropy of the original fracture.

Acknowledgements

A scholarship from the China Scholarship Council for the first author is acknowledged. Support from CSIRO Energy is acknowledged. The financial support from the National Natural Science Foundation of China under Grant no. 413200104005 is acknowledged. Drishiti software developed by Australian National University is also acknowledged.

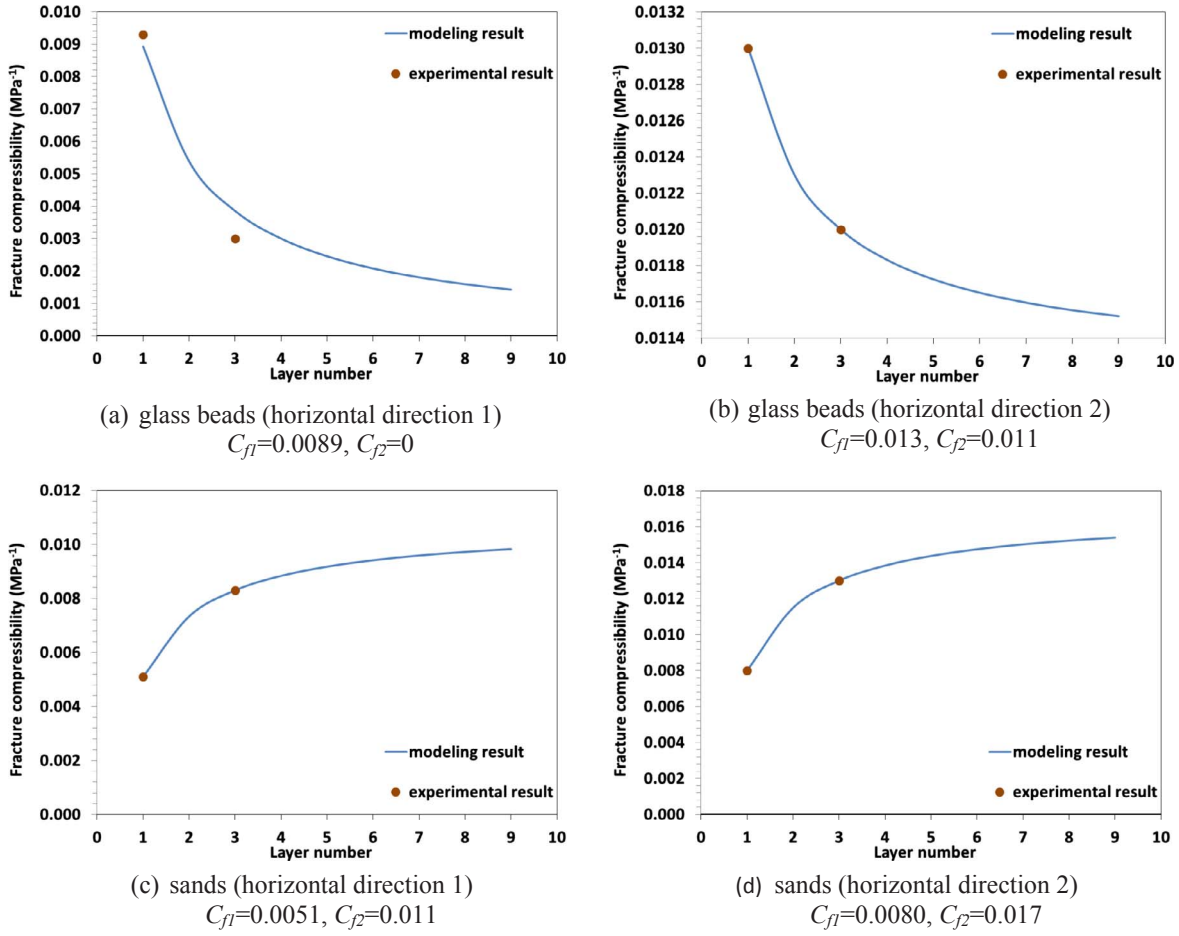

(a) glass beads (horizontal direction 1) C_{f1}=0.0089, C_{f2}=0

(b) glass beads (horizontal direction 2) C_{f1}=0.013, C_{f2}=0.011

(c) sands (horizontal direction 1) C_{f1}=0.0051, C_{f2}=0.011

(d) sands (horizontal direction 2) C_{f1}=0.0080, C_{f2}=0.017

Fig. 14. Fracture compressibility modelling results.

References

[1] EIA. 2016. Shale Gas Production. https://www.eia.gov/dnav/ng/ng_prod_shalegas_s1_a.htm.

[2] EIA. 2016. U.S. natural gas production reaches record high in 2015. https://www.eia.gov/todayinenergy/detail.php?id=25832.

[3] Vidic RD, Brantley SL, Vandenbossche JM, Yoxtheimer D, Abad JD. Impact of shale gas development on regional water quality. Science 2013;340(6134):826–37.

[4] Wang Q, Li R. Research status of shale gas: a review. Renew Sustain Energy Rev 2017;74:715–20.

[5] Estrada JM, Bhamidimarri R. A review of the issues and treatment options for wastewater from shale gas extraction by hydraulic fracturing. Fuel 2016;182:292–303.

[6] Cai J, Wei W, Hu X, Liu R, Wang J. Fractal characterization of dynamic fracture network extension in porous media. Fractals. 2017;25(2):1750023.

[7] Wei W, Xia Y. Geometrical, fractal and hydraulic properties of fractured reservoirs: a mini-review. Adv Geo-Energy Res 2017;1(1):31–8.

[8] Zhou T, Zhang S, Yang L, Ma X, Zou Y, Lin H. Experimental investigation on fracture surface strength softening induced by fracturing fluid imbibition and its impacts on flow conductivity in shale reservoirs. J Nat Gas Sci Eng 2016;36(Part A):893–905.

[9] Yang L, Ge H, Shen Y, Zhang J, Yan W, Wu S, et al. Imbibition inducing tensile fractures and its influence on in-situ stress analyses: a case study of shale gas drilling. J Nat Gas Sci Eng 2015;26:927–39.

[10] Hou T, Zhang S, Ma X, Shao J, He Y, Lv X, et al. Experimental and theoretical study of fracture conductivity with heterogeneous proppant placement. J Nat Gas Sci Eng 2017;37:449–61.

[11] Zhang J, Kamenov A, Zhu D, Hill AD. Measurement of realistic fracture conductivity in the Barnett shale. J Unconventional Oil Gas Resour 2015;11:44–52.

[12] Akbari M, Javad Ameri M, Kharazmi S, Motamedi Y, Pournik M. New correlations to predict fracture conductivity based on the rock strength. J Petrol Sci Eng 2017;152:416–26.

[13] Yao S, Zeng F, Liu H. A semi-analytical model for hydraulically fractured wells with stress-sensitive conductivities. In: SPE Unconventional Resources Conference-Canada, 5–7 November, Calgary, Alberta, Canada: SPE 167230; 2013.

[14] Tan Y, Pan Z, Liu J, Wu Y, Haque A, Connell LD. Experimental study of permeability and its anisotropy for shale fracture supported with proppant. J Nat Gas Sci Eng 2017;44:250–64.

[15] Mollanouri Shamsi MM, Farhadi Nia S, Jessen K. Dynamic conductivity of proppant-filled fractures. J Petrol Sci Eng 2016;151:183–93.

[16] Wen Q, Zhang S, Wang L, Liu Y, Li X. The effect of proppant embedment upon the long-term conductivity of fractures. J Petrol Sci Eng 2007;55(3–4):221–7.

[17] Fredd CN, McConnell SB, Boney CL, England KW. Experimental study of hydraulic fracture conductivity demonstrates the benefits of using proppants. In: SPE Rocky Mountain Regional/Low Permeability Reservoirs Symposium, 12–15 March, Denver, CO, America: SPE 60326; 2000.

[18] Wu Y, Pan Z, Zhang D, Down DI, Lu Z, Connell LD. Experimental study of permeability behaviour for proppant supported coal fracture. J Nat Gas Sci Eng 2018;51:18–26.

[19] Kassis S, Sondergeld CH. Fracture permeability of gas shale: effects of roughness, proppant, fracture offset, and confining pressure. In: SPE International Oil & Gas Conference and Exhibition, 8–10 June, Beijing, China: SPE 131376; 2010.

[20] Cao H, Yi X, Lu Y, Xiao Y. A fractal analysis of fracture conductivity considering the effects of closure stress. J Nat Gas Sci Eng 2016;32:549–55.

[21] Bortolan Neto L, Khanna A, Kotousov A. Conductivity and performance of hydraulic fractures partially filled with compressible proppant packs. Int J Rock Mech Min Sci 2015;74:1–9.

[22] Zhang J, Zhu D, Hill AD. A new theoretical method to calculate shale fracture conductivity based on the population balance equation. J Petrol Sci Eng 2015;134:40–8.

[23] Khanna A, Kotousov A, Sobey J, Weller P. Conductivity of narrow fractures filled with a proppant monolayer. J Petrol Sci Eng 2012;100:9–13.

[24] Wan Y, Pan Z, Tang S, Connell LD, Down DD, Camilleri M. An experimental investigation of diffusivity and porosity anisotropy of a Chinese gas shale. J Nat Gas Sci Eng 2015;23:70–9.

[25] Pan Z, Ma Y, Connell LD, Down DI, Camilleri M. Measuring anisotropic permeability using a cubic shale sample in a triaxial cell. J Nat Gas Sci Eng 2015;26:336–44.

[26] Brace W, Walsh JB, Frangos WT. Permeability of granite under high pressure. J Geophys Res 1968;73(6):2225–36.

[27] Ghanizadeh A, Amann-Hildenbrand A, Gasparik M, Gensterblum Y, Krooss BM, Littke R. Experimental study of fluid transport processes in the matrix system of the European organic-rich shales: II. Posidonia Shale (Lower Toarcian, northern Germany). Int J Coal Geol 2014;123:20–33.

[28] Pan Z, Connell LD, Camilleri M. Laboratory characterisation of coal reservoir permeability for primary and enhanced coalbed methane recovery. Int J Coal Geol 2010;82(3–4):252–61.

[29] Sander R, Pan Z, Connell LD. Laboratory measurement of low permeability

unconventional gas reservoir rocks: a review of experimental methods. J Nat Gas Sci Eng 2017;37:248–79.
[30] Ma Y, Pan Z, Zhong N, Connell LD, Down DI, Lin W, et al. Experimental study of anisotropic gas permeability and its relationship with fracture structure of Longmaxi Shales, Sichuan Basin, China. Fuel 2016;180:106–15.
[31] Mckee CR, Bumb AC, Koenlg RA. Stress-dependent permeability and porosity of coal and other geologic formations. SPE Form Eval 1988:81–91. March.
[32] Yang B, Kang Y, Li X, You L, Chen M. An integrated method of measuring gas permeability and diffusion coefficient simultaneously via pressure decay tests in shale. Int J Coal Geol 2017;179:1–10.
[33] Nimmo JR. Porosity and pore size distribution. Encyclopedia of soils in the environment. 3. London: Elsevier; 2004. 295–303.
[34] Parker M, Glasbergen G, van Batenburg D, Weaver J, Slabaugh B. High-porosity fractures yield high conductivity. In: SPE Annual Technical Conference and Exhibition, , 9–12 October, Dallas, Texas, USA: SPE 96848; 2005.
[35] Glover P. Petrophysics MSc Course Notes, Chapter 2. Porosity; 2014. (http://homepages.see.leeds.ac.uk/~earpwjg/PG_EN/CD%20Contents/GGL-66565%20Petrophysics%20English/Chapter%202.PDF).
[36] Bhandari AR, Flemings PB, Polito PJ, Cronin MB, Bryant SL. Anisotropy and stress dependence of permeability in the Barnett Shale. Transp Porous Media 2015;108(2):393–411.
[37] Chalmers GR, Ross DJ, Bustin RM. Geological controls on matrix permeability of Devonian Gas Shales in the Horn River and Liard basins, northeastern British Columbia, Canada. J Coal Geol 2012;103:120–31.
[38] Bolton AJ, Maltman AJ, Fisher Q. Anisotropic permeability and bimodal pore size distributions of fine-grained marine sediments. Mar Pet Geol 2000;17(6):657–72.